

# Squeezing of quantum noise of motion in a micromechanical resonator

J.-M. Pirkkalainen<sup>1</sup>, E. Damskäg<sup>1</sup>, M. Brandt<sup>1</sup>, F. Massel<sup>2</sup>, and M. A. Sillanpää<sup>1\*</sup>

<sup>1</sup>*Department of Applied Physics, Aalto University, PO Box 11100, FI-00076 Aalto, Finland.*

<sup>2</sup>*University of Jyväskylä, Department of Physics, Nanoscience Center, University of Jyväskylä, PO Box 35 (YFL) FI-40014 University of Jyväskylä, Jyväskylä, Finland.*

A pair of conjugate observables, such as the quadrature amplitudes of harmonic motion, have fundamental fluctuations which are bound by the Heisenberg uncertainty relation. However, in a squeezed quantum state, fluctuations of a quantity can be reduced below the standard quantum limit, at the cost of increased fluctuations of the conjugate variable. Here we prepare a nearly macroscopic moving body, realized as a micromechanical resonator, in a squeezed quantum state. We obtain squeezing of one quadrature amplitude  $1.4 \pm 0.5$  dB below the standard quantum limit, thus achieving a long-standing goal of obtaining motional squeezing in a macroscopic object.

The motion  $x(t) = X_1(t) \cos(\omega_m t) + X_2(t) \sin(\omega_m t)$  of a harmonic oscillator having the natural oscillating frequency  $\omega_m$  can be described by the quadrature amplitudes  $X_1$  and  $X_2$  which have slow fluctuations. The fluctuations, presented in units of the quantum zero-point fluctuation amplitude  $x_{zp}$ , satisfy the Heisenberg uncertainty relation  $\Delta X_1 \Delta X_2 \geq 1$ . One of the two can be prepared (=squeezed) below the value 1, at the expense of increased fluctuations in the other quadrature. In optics, squeezing of laser light was observed in early 80's [1, 2], not long after the possibility was realized. One motivation for the study of squeezed quantum states is the possibility to measure without the imprecision due to the zero-point fluctuations [3].

Superconducting microcircuits were the first systems with a nearly macroscopic degree of freedom where squeezing was demonstrated [4]. It has been a formidable challenge to obtain squeezing in the motional state of a macroscopic object. The possibility of squeezing in gravitational antennae has been hypothesized a long time ago [5, 6], but technological limitations have thus far prohibited experimental evidence. Other quantum-mechanical phenomena on large oscillators [7, 8], on the other hand, have been actively investigated recently in the cavity optomechanics setting coupling electromagnetic cavity mode and the oscillator motion [9]. Output of squeezed light [10–12] was recently observed, but this does not yet imply the oscillator mode is squeezed.

Here we report the first discovery of squeezing of the motional state of a nearly macroscopic body, realized as a micromechanical resonator measuring 15 microns in diameter. We utilize the novel idea of dissipative squeezing [13, 14], see Fig. 1 a, where the system is allowed to cool towards a squeezed low-energy state. This method has the great advantage of being able to create unconditional squeezing in the steady-state. This contrasts to many other plausible methods of squeezing generation [15–21]. Our approach is closely related to the quantum non-demolition measurements [22–24] which, however, are not able to generate true squeezing without feedback. At this point we mention that classical squeezing of thermal noise is routinely observed in mechanical systems [25–27].

The mechanical element (Fig. 1 b) is a drum resonator basically similar to Refs. 28, 29. The 120 nm thick Al drum is capacitively connected to the cavity (Fig. 1 c) consisting of a meandering superconducting Al strip. This kind of microwave optomechanical systems are conveniently described using a model involving lumped electromagnetic elements. The interaction between the microwave cavity and the mechanical vibrations is given by the energy  $g_0 n_P x$ , where  $n_P$  is the number of photons externally applied by microwave pump(s), and  $g_0$  is the radiation-pressure coupling energy. Because usually  $g_0$  is much smaller than other energy scales, a large  $n_P \gg 1$  is needed to effectively enhance the interaction up to a value  $G = g_0 \sqrt{n_P}$ . If the pump is applied at the frequency  $\omega_- = \omega_c - \omega_m$  (the red sideband), the physics leads to sideband cooling of the mechanical vibrations, possibly down to the quantum ground state [29, 30].

The scheme of Ref. [13] requires two pump microwaves, one applied at the red sideband, and the other at the blue sideband frequency  $\omega_+ = \omega_c + \omega_m$  (Fig. 1 d). The two pertinent effective couplings are called  $G_-$  and  $G_+$ , respectively. This setup can be described as sideband cooling of a Bogoliubov (BG) mode [13, 31]. In laboratory frame, this corresponds to cooling the mechanical mode towards a squeezed vacuum state. The BG mode couples to the cavity with the coupling energy  $G_\beta = \sqrt{G_-^2 - G_+^2}$ . Although an arbitrary squeezing ratio can be selected by tuning the ratio  $G_-/G_+$ , an optimum is found typically around  $G_-/G_+ \sim 1.4$ .

The measurements are carried out inside a Bluefors dry dilution refrigerator in the temperature interval 7 mK ... 200 mK. The cavity is first characterized having the frequency  $\omega_c/2\pi \simeq 6.9004$  GHz, and coupled to the transmission lines with the decay rates  $\kappa_{Ei}/2\pi \simeq 50$  kHz,  $\kappa_{Eo}/2\pi \simeq 270$  kHz through the input and output ports, respectively. The internal losses are characterized by the rate  $\kappa_I/2\pi \simeq 330$  kHz, and the total cavity damping rate is  $\kappa = \kappa_{Ei} + \kappa_{Eo} + \kappa_I \simeq (2\pi) \cdot 650$  kHz. We operate in the good cavity limit  $\omega_m/\kappa \simeq 20 \gg 1$ , a prerequisite for efficient sideband cooling and squeezing generation.

The mechanical resonator is characterized using a sin-

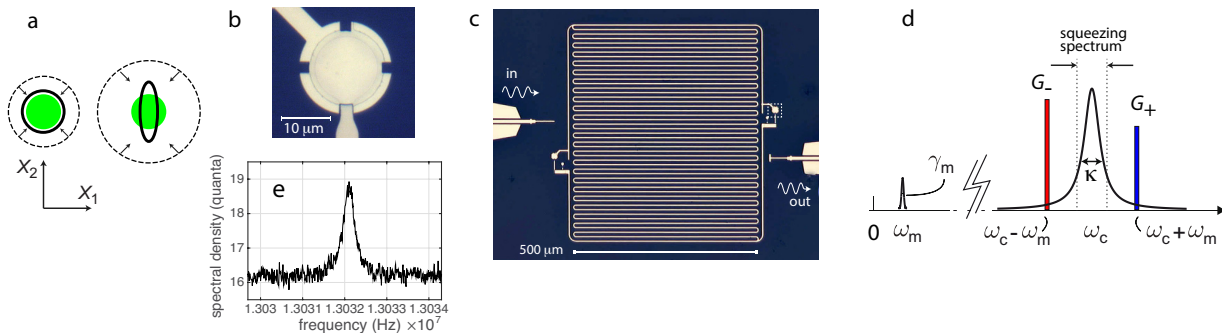


FIG. 1: *Setup of the microwave optomechanical squeezing experiment.* (a), Idea of dissipative squeezing. The initial fluctuation amplitudes of the quadratures are marked with dashed lines, and the final ones with solid lines. The green circles denote the quantum ground state. In sideband cooling (left), the initial fluctuations uniformly cool towards the ground state. Right, in a suitably engineered system, cooling can be quadrature-dependent, hence leading to one quadrature becoming squeezed. (b), (c), Optical micrographs of the micromechanical device and of the cavity. There are two drum resonators connected to cavity, however, only one of them (within the dashed rectangle) is operated. The cavity is asymmetrically coupled to the input port (left), and to the output port (right) for transmission measurements. (d), The frequencies involved in the scheme. The cavity is pumped by two nonequal-amplitude microwave tones at the sideband frequencies  $\omega_{\pm} = \omega_c \pm \omega_m$ . (e) Example of the thermal motion signal measured at the refrigerator base temperature, with the coupling  $G_-/2\pi \simeq 1.3$  kHz.

gle pump tone at the red sideband. The emission at the cavity frequency then shows the usual thermal motion peak at the motional sideband at a frequency  $\omega_m/2\pi \simeq 13.032$  MHz above the pump. We can extract the intrinsic linewidth of the mechanics  $\gamma_m/2\pi \simeq 330$  Hz corresponding to the  $Q$ -value  $Q_m \simeq 3.9 \times 10^4$  from the data as in Fig. 1 e. Although  $Q_m$  is lower than in e.g. Refs. 24, 28, 29, this can be in fact beneficial for this experiment due to the mitigation of parametric instabilities [23, 31]. A narrow vacuum gap  $\sim 70$  nm between the drum and a bottom electrode allows for a relatively large single-photon coupling energy  $g_0/2\pi \simeq 90$  Hz.

An important benchmarking for cavity optomechanical experiments is how well the mechanical mode thermalizes to the temperature  $T$  of the refrigerator. Here we observe the linear temperature dependence expected (as seen in Fig. 2 a) in equilibrium,  $k_B T = n_m^T \hbar \omega_m$  down to  $\simeq 25$  mK. Here,  $n_m^T$  is the equilibrium thermal phonon number defined accordingly. In the further experiment, we operate at the minimum  $T$  where we know that the mechanical mode is at 25 mK corresponding to  $n_m^T \simeq 40$  at low pump powers.

We proceed with a series of further checks and calibrations on the way towards demonstrating squeezing. Next we perform a regular sideband cooling experiment ( $G_+ = 0$ ), see e.g. Refs. [32–36]. The measured spectral density is shown by the black symbols in Fig. 2 b-e, overlaid with theoretical predictions from the standard formalism using input-output theory [31]. For the plot, we have subtracted a large background level due to the amplifier noise, hence displaying only the signal part due to the sample. The mechanical mode cools down to a thermal occupation  $n_m \simeq 0.38$  ( $n_m = 0$  corresponds here to the ground state). The double peak seen in Fig. 2

e signifies the onset of the strong-coupling regime when  $G_- \sim \kappa$ . The vertical scale of the data is used as an adjustable parameter, common to all data. This is because the vertical scale is set by the amplification gain which is difficult to tell accurately enough. The data is plotted in dimensionless units (quanta) which is the natural unit from the theory point of view.

Given that we can cool the drum motion close to the ground state provides a promising starting point for creating squeezed motional states. We switch on the blue pump while keeping the red on, obeying  $G_- > G_+$  for stability. This creates a certain BG mode depending on the ratio  $G_-/G_+$ . In order to ascertain which BG mode we have, we calibrate the input line attenuations separately for both pump generators. We choose very low pump powers such that the damping rate due to either pump,  $\gamma_{\pm} = 4G_{\pm}^2/\kappa \ll \gamma_m$  and adjust the powers such that we obtain equal response due to either pump. The imprecision for setting equal response is estimated to be  $\pm 0.2$  dB which is also the imprecision for constructing a given BG mode.

Next we discuss a specific BG mode obeying  $G_-/G_+ \simeq 1.52$  which is expected to represent a choice close to optimum. At the lowest pump powers, the back-action cooling is negligible and we reveal the bare BG mode undressed from the cavity. Under this condition, the equilibrium BG mode occupancy  $n_{BG}^T$  is expected to follow a linear temperature dependence same way as the mechanical mode, but with an elevated temperature [31]. More relevant than  $n_{BG}^T$ , however, is the agreement of the spectra with theoretical prediction, which here is connected to the area under the Lorentzian BG mode peak. We test this in Fig. 2 a and observe an excellent agreement to the theory. The green solid line is an expectation based on

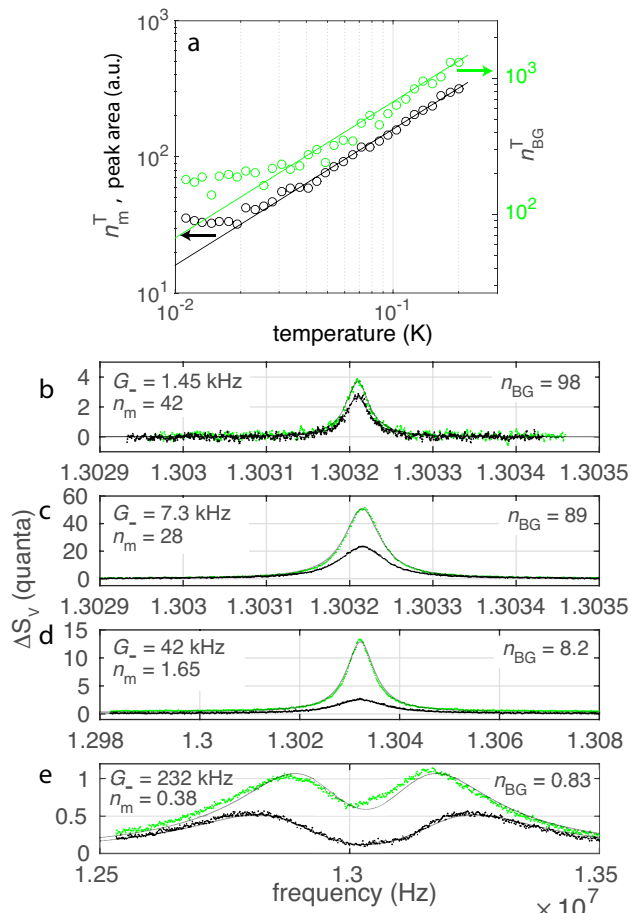


FIG. 2: *Cooling the Bogoliubov mode.* In all the panels, black color refers to regular sideband cooling (i.e.,  $G_+ = 0$ ) used as calibration, whereas green refers to the BG mode experiment. (a), Thermalization in equilibrium. The left scale gives  $n_m^T$ , as well as the area of both the sideband cooling peaks, and of the BG mode peaks (both in a.u.), whereas the right hand side scale is  $n_{BG}^T$ . (b)-(e), Output spectrum during sideband cooling (black), or under BG mode conditions (green). The solid lines are theoretical curves. The  $n_m$  values refer to the  $G_+ = 0$  case.

the calibrated  $G_-/G_+$  ratio, and on the  $G_+ = 0$  data.

Next, we increase the effective couplings. Plotted in conjunction with the sideband cooling data, in Fig. 2 b-e we display the BG mode spectra in green. The theoretical plots show a good agreement to the data. In Fig. 2 e, the BG mode curve is slightly shifted to the left probably because of an energy-dependent shift in the cavity frequency. When using fixed pump frequencies as here, the cavity can become slightly detuned at certain pump powers. Here we have used as adjustable parameters the bath temperatures of both the cavity and the mechanics. Both baths heat up with the pump powers, for the BG mode up to  $n_I \simeq 0.74$ ,  $n_m^T \simeq 86$  (instead of  $n_{BG}^T$ , we prefer to quantify the bath with  $n_m^T$ ) in Fig. 2 e, which is attributed to dielectric heating. These factors together

set the limits for the cooling as well as squeezing. As one can anticipate, the baths heat up more if we apply both pumps instead of only one.

In Fig. 2 b-e we label the fitted values of the BG mode occupation  $n_{BG}$  which is a quantity analogous to  $n_m$  in case of regular sideband cooling. Although  $n_{BG}$  is somewhat secondary quantity, a value  $n_{BG} < 1$  as obtained in Fig. 2 e indicates squeezing. More precisely we can evaluate the amount of squeezing by evaluating the quadrature variances [31]. This way, we obtain that the mechanical mode is squeezed below vacuum, in Fig. 2 e by  $\simeq 1.4$  dB.

The best verification of squeezing comes from the quadrature spectra which amount to tomography of the state. We digitally mix down the signal using the center frequency  $\omega_c$  of the pumps as a local oscillator (LO), hence making homodyne detection. The quadrature spectra show strong dependence on the LO phase. We identify the minimum emission as the  $X_1$  quadrature, and the maximum, offset by  $90^\circ$ , as  $X_2$ . In Fig. 3 we show the corresponding quadrature spectra  $S_1$  and  $S_2$  together with the total spectrum (the BG mode) and the cooling spectrum. We plot the quantities  $2S_1$  and  $2S_2$  for more conveniently presenting them together with the other two curves. The theoretical predictions overlaid on the data show an excellent agreement. In the best case of Fig. 3 d, the motion of the mechanical resonator has been squeezed about 1.4 dB below the Heisenberg limit. When varying the LO phase, we also observe an excellent agreement to theory (Fig. 4). The bath temperatures are found to be slightly enhanced over to the previous dataset in Fig. 2 [31]. We also find that this data agrees with a slightly shifted BG ratio  $G_-/G_+ \simeq 1.43$  which is attributed to drift in the tunable filters at room temperature over the about one week after the calibration.

We now discuss an issue which is critical for understanding the quadrature spectra, namely, parametric effects beyond the ideal optomechanical model. One can satisfactorily model the total BG mode spectrum (and get equal squeezing) without imposing any parametric modulation [31], however, the quadratures show much more phase dependence than predicted. In the scheme, mixing products of the pumps can appear both at  $2\omega_m$  as well as  $2\omega_c$ , the frequencies most susceptible to cause parametric modulation via e.g. thermal effects [23, 31]. We theoretically explored with parametric modulation of  $\omega_m$ , however, strong phase dependence could not be created. Instead, modulation of  $\omega_c$  out of phase with respect to the pumps gives an excellent match to the quadratures with the values quoted in Fig. 3. The excellent agreement to the data strongly suggests the model captures the physics. The weak dependence of the modulation depth on the pump powers indicates a thermal effect which gets weaker when temperatures grow and thermal contact improves.

Although the parametric effects have a dramatic influence on the quadratures of the output spectrum, they

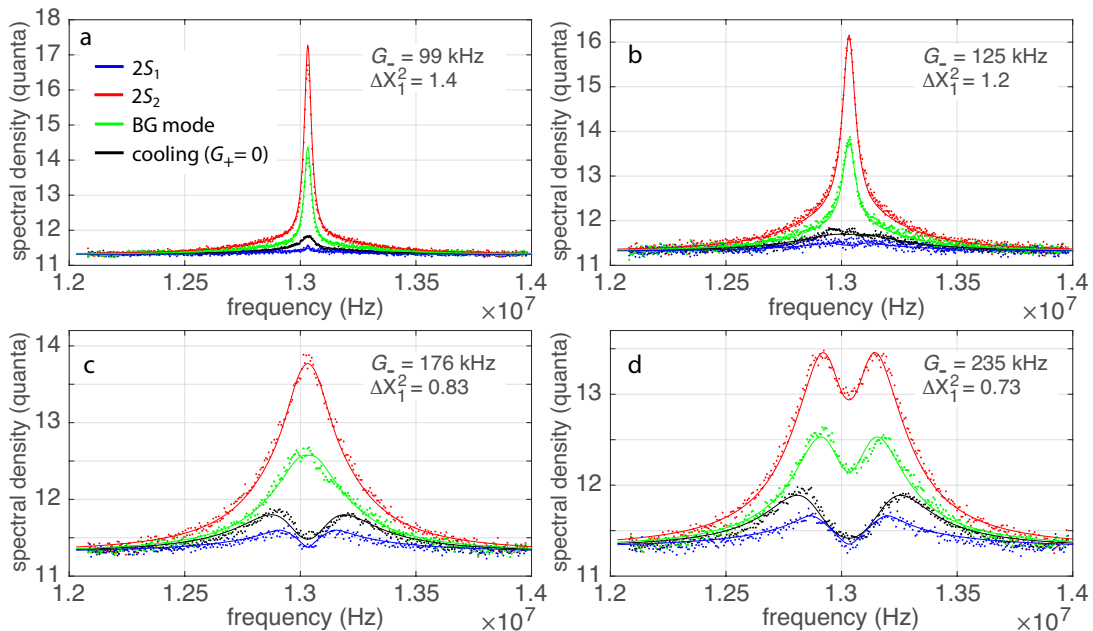


FIG. 3: *Squeezing deduced from the quadrature spectra.* In all panels, blue and red refer to the cold and hot quadratures  $X_1$  and  $X_2$ , respectively. Black and green refer to the regular sideband cooling, and the BG mode, respectively. The solid lines are theory curves. The pump powers are increased from (a) to (d) as marked in the panels while  $G_-/G_+ \simeq 1.43$  ratio is kept constant. The variances  $\Delta X_1^2$  are marked, and a value less than one implies squeezing below vacuum. The amplitudes of parametric modulation to the cavity are  $\epsilon_c/2\pi \simeq 35, 48, 49, 56$  kHz from (a) to (d).

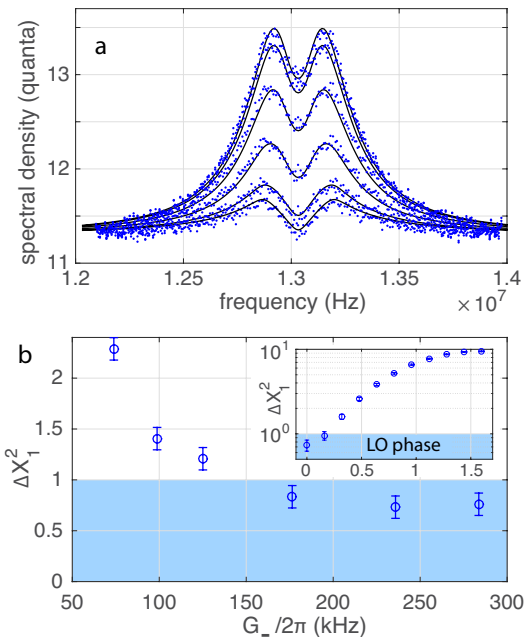


FIG. 4: *Tomography and final results.* (a), The quadrature data similar to Fig. 3 d, plotted at different LO phase values at  $\pi/10$  steps from 0 to  $\pi/2$ , from bottom to top. (b), The  $X_1$  quadrature variance as a function of pump power. The blue region signifies squeezing below the quantum limit. The inset shows the quadrature variance from the data in (a).

only weakly affect the squeezing of the mechanics, in the present case we find a reduction by about 10 %. The shapes of the spectra, in turn, are sensitive to most parameters,  $n_m^T$  and  $n_I$  in particular. Moreover, squeezing is somewhat insensitive to any parameters, including the parametric modulation, in the present parameter region. This provides a solid foundation for the claims. The final numbers are quoted in Fig. 4 b.

In conclusion, we have achieved the reduction of the quantum fluctuations in a nearly macroscopic moving object below the "sound of silence" level by 1.4 dB in one quadrature. Following the discoveries of ground-state cooling [7, 29, 30], observation of zero-point fluctuations in mechanical systems [37], and entanglement [8], our work goes forward to establish the reality of another fundamental quantum property in moving objects.

Note added: while finalizing the paper, we became aware of a similar experiment [38].

\* Mika.Sillanpaa@aalto.fi

- [1] D. F. Walls, *Nature* **306**, 141 (1983).
- [2] R. E. Slusher, L. W. Hollberg, B. Yurke, J. C. Mertz, and J. F. Valley, *Phys. Rev. Lett.* **55**, 2409 (1985).
- [3] The LIGO Scientific Collaboration, *Nature Physics* **7**, 962 (2011).
- [4] B. Yurke, P. Kaminsky, R. Miller, E. Whittaker, A. Smith, A. Silver, and R. Simon, *Phys. Rev. Lett.* **60**,

- 764 (1988).
- [5] J. N. Hollenhorst, Phys. Rev. D **19**, 1669 (1979).
- [6] L. P. Grishchuk and M. V. Sazhin, Sov. Phys. JETP **57**, 1128 (1983).
- [7] A. D. O’Connell, M. Hofheinz, M. Ansmann, R. C. Bialczak, M. Lenander, E. Lucero, M. Neeley, D. Sank, H. Wang, M. Weides, et al., Nature **464**, 697 (2010).
- [8] T. A. Palomaki, J. D. Teufel, R. W. Simmonds, and K. W. Lehnert, Science **342**, 710 (2013).
- [9] M. Aspelmeyer, T. J. Kippenberg, and F. Marquardt, Rev. Mod. Phys. **86**, 1391 (2014).
- [10] D. W. C. Brooks, T. Botter, S. Schreppler, T. P. Purdy, N. Brahms, and D. M. Stamper-Kurn, Nature **488**, 476 (2012).
- [11] A. H. Safavi-Naeini, S. Groblacher, J. T. Hill, J. Chan, M. Aspelmeyer, and O. Painter, Nature **500**, 185 (2013).
- [12] T. P. Purdy, P.-L. Yu, R. W. Peterson, N. S. Kampel, and C. A. Regal, Phys. Rev. X **3**, 031012 (2013).
- [13] A. Kronwald, F. Marquardt, and A. A. Clerk, Phys. Rev. A **88**, 063833 (2013).
- [14] H. Tan, G. Li, and P. Meystre, Phys. Rev. A **87**, 033829 (2013).
- [15] M. Blencowe and M. Wybourne, Physica B: Condensed Matter **280**, 555 (2000).
- [16] M. J. Woolley, A. C. Doherty, G. J. Milburn, and K. C. Schwab, Phys. Rev. A **78**, 062303 (2008).
- [17] A. A. Clerk, F. Marquardt, and K. Jacobs, New Journal of Physics **10**, 095010 (2008).
- [18] L. Tian, M. S. Allman, and R. W. Simmonds, New Journal of Physics **10**, 115001 (2008).
- [19] K. Jähne, C. Genes, K. Hammerer, M. Wallquist, E. S. Polzik, and P. Zoller, Phys. Rev. A **79**, 063819 (2009).
- [20] A. Szorkovszky, A. C. Doherty, G. I. Harris, and W. P. Bowen, Phys. Rev. Lett. **107**, 213603 (2011).
- [21] G. Vasilakis, H. Shen, K. Jensen, M. Balabas, D. Salart, B. Chen, and E. S. Polzik, Nat Phys **11**, 389 (2015).
- [22] J. B. Hertzberg, T. Rocheleau, T. Ndukum, M. Savva, A. A. Clerk, and K. C. Schwab, Nature Physics **6**, 213 (2010).
- [23] J. Suh, M. D. Shaw, H. G. LeDuc, A. J. Weinstein, and K. C. Schwab, Nano Letters **12**, 6260 (2012).
- [24] J. Suh, A. J. Weinstein, C. U. Lei, E. E. Wollman, S. K. Steinke, P. Meystre, A. A. Clerk, and K. C. Schwab, Science **344**, 1262 (2014).
- [25] D. Rugar and P. Grütter, Phys. Rev. Lett. **67**, 699 (1991).
- [26] R. Almog, S. Zaitsev, O. Shtempluck, and E. Buks, Phys. Rev. Lett. **98**, 078103 (2007).
- [27] I. Mahboob, H. Okamoto, K. Onomitsu, and H. Yamaguchi, Phys. Rev. Lett. **113**, 167203 (2014).
- [28] J. D. Teufel, D. Li, M. S. Allman, K. Cicak, A. J. Sirois, J. D. Whittaker, and R. W. Simmonds, Nature **471**, 204 (2011).
- [29] J. D. Teufel, T. Donner, D. Li, J. W. Harlow, M. S. Allman, K. Cicak, A. J. Sirois, J. D. Whittaker, K. W. Lehnert, and R. W. Simmonds, Nature **475**, 359 (2011).
- [30] J. Chan, T. P. M. Alegre, A. H. Safavi-Naeini, J. T. Hill, A. Krause, S. Gröblacher, M. Aspelmeyer, and O. Painter, Nature **478**, 89 (2011).
- [31] See Supplementary Materials.
- [32] S. Gigan, H. R. Boehm, M. Paternostro, F. Blaser, G. Langer, J. B. Hertzberg, K. C. Schwab, D. Baeuerle, M. Aspelmeyer, and A. Zeilinger, Nature **444**, 67 (2006).
- [33] A. Schliesser, P. Del’Haye, N. Nooshi, K. J. Vahala, and T. J. Kippenberg, Phys. Rev. Lett. **97**, 243905 (2006).
- [34] T. Rocheleau, T. Ndukum, C. Macklin, J. B. Hertzberg, A. A. Clerk, and K. C. Schwab, Nature **463**, 72 (2010).
- [35] F. Massel, S. U. Cho, J.-M. Pirkkalainen, P. J. Hakonen, T. T. Heikkilä, and M. A. Sillanpää, Nat. Commun. **3**, 987 (2012).
- [36] X. Song, M. Oksanen, J. Li, P. J. Hakonen, and M. A. Sillanpää, Phys. Rev. Lett. **113**, 027404 (2014).
- [37] A. H. Safavi-Naeini, J. Chan, J. T. Hill, T. P. M. Alegre, A. Krause, and O. Painter, Phys. Rev. Lett. **108**, 033602 (2012).
- [38] Schwab group, to be published (2015).

**Acknowledgements** We would like to thank Pasi Lähteenmäki, Tero Heikkilä and André Xuereb for useful discussions. This work was supported by the Academy of Finland (contract 250280, CoE LTQ, 275245) and by the European Research Council (240387-NEMSQED, 240362-Heatronics, 615755-CAVITYQPD). The work benefited from the facilities at the Micronova Nanofabrication Center and at the Low Temperature Laboratory infrastructure.

# Supplementary Information for "Squeezing of quantum noise of motion in a micromechanical resonator"

J.-M. Pirkkalainen<sup>1</sup> E. Damskagg<sup>1</sup> M. Brandt<sup>1</sup> F. Massel<sup>2</sup> M. A. Sillanpää<sup>1</sup>

<sup>1</sup>Department of Applied Physics, Aalto University, PO Box 11100, FI-00076 Aalto, Finland.

<sup>2</sup>University of Jyväskylä, Department of Physics, Nanoscience Center, University of Jyväskylä, PO Box 35 (YFL) FI-40014 University of Jyväskylä, Jyväskylä, Finland.

## DEVICE FABRICATION

As displayed in Fig. 5, the sample fabrication consists of three layers of electron-beam lithography on a quartz substrate. First, the bottom electrode below the drum is patterned (A,B), and aluminium with thickness of 20 nm is deposited by e-beam evaporation (C). A sacrificial layer made with amorphous silicon (a-Si) is deposited using PECVD (D). The gases used are SiH<sub>4</sub> at the flow rate of 14 sccm, and He with the rate 266 sccm. We use the deposition pressure of 2000 mTorr, temperature of 200 C°, and 10 W of forward power. The deposition time is 2 min 30 sec, resulting in about 70 nm layer of a-Si verified with AFM. The following lithography is used to define a PMMA resist etch mask for the sacrificial layer on top of the bottom electrode (E). The a-Si layer is removed (F) from other areas beside the etching mask with reactive ion etching (RIE) using a SF<sub>6</sub> flow rate 100 sccm at 45 mTorr pressure, and a forward power of 100 W for the time of 1 min 20 sec. After etching, the etch mask is removed in RIE using 45 sccm of O<sub>2</sub> and 20 sccm of Ar at 250 mTorr pressure and forward power of 50 W for 5 min. The top layer containing the cavity and the drum is patterned by lithography (G) and a 120 nm thickness of aluminium is evaporated on top of the substrate (H). A galvanic contact between the bottom electrode and the cavity does not arise owing to the native Al oxide, however, a large capacitance of the oxide contact results in a short circuit contact at the relevant high microwave frequencies. It could be the dirty native oxide layer causes the somewhat high internal losses of the cavity. After lift-off in acetone, the mechanical resonator is released by etching away the a-Si sacrificial layer using RIE with a nearly isotropic SF<sub>6</sub> etch (I). In order to prevent the chip from heating during the etching, etching is done in periods of 1 min, with 2 min breaks in between. Totally, the release etch takes 30 min, completely removing the a-Si layer under the resonator.

## EXPERIMENTAL SETUP

We first mention how the microwave optomechanical device can be simply described using lumped electromagnetic elements (see Fig. 6). The motion of the drum changes its capacitance  $C_g(x)$ . The total capacitance of the cavity can be summed up as a constant  $C$  and an  $x$ -dependent part  $C_g(x)$ . The frequency of this cavity hence is

$$\omega_c = \frac{1}{\sqrt{L(C + C_g(x))}}. \quad (1)$$

Linearization gives the coupling

$$g_0 = \frac{\partial \omega_c}{\partial x} x_{z\text{p}} = \frac{\omega_c}{2C} \left( \frac{\partial C_g}{\partial x} \right) x_{z\text{p}}. \quad (2)$$

Modeling the device layout using electromagnetic simulation software gives the equivalent parameters  $C \sim 16$  fF,  $L \sim 14$  nH. It is beneficial to get as low  $C$  as possible in order to maximize coupling. Here the role of quartz substrate is critical because it has a low dielectric constant  $\epsilon_r \sim 4$  as compared to sapphire or silicon ( $\epsilon_r \sim 10 \dots 12$ ). This difference amounts to a factor of two in  $C$ . The input and output coupling rates are also simulated in the actual device structure.

We use a pulse-tube powered Bluefors "dry" dilution refrigerator to cool the device down to about 7 mK. Inside the cryostat, the incoming pump signal is attenuated at all temperature stages by a total of about 40 dB (including cabling) in order to dampen the Johnson noise from higher temperatures. We used relatively small-valued attenuators at the two lowest temperature stages in order to avoid heating the refrigerator by the pump microwaves. However, one can check that the input noise  $n_i$ , see Eq. (19), (considering an ideal setting) is only a vanishing amount above

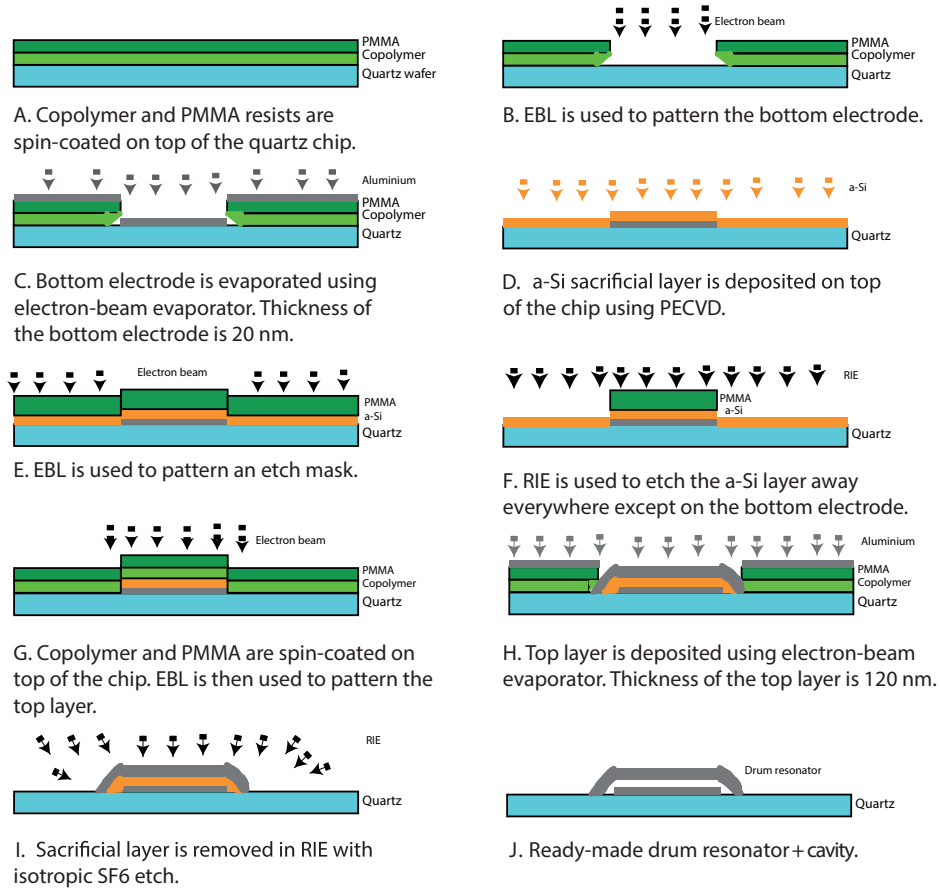


FIG. 5: *Detailed device fabrication process.* For discussion, see text.

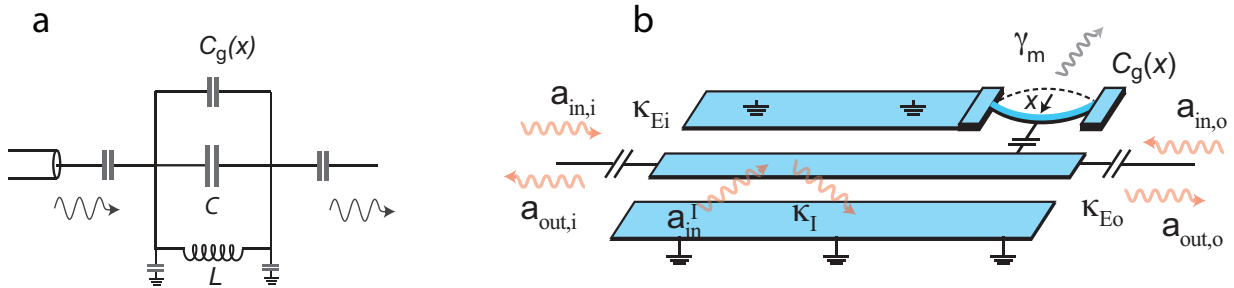


FIG. 6: *Schematics of the microwave optomechanical device.* (a), Model in terms of lumped electromagnetic elements. (b), Modeling scheme in the input-output theory. The cavity is exposed to noise from both the input (subscripts  $i$ ) and output (subscripts  $o$ ) couplers, as well as from the internal losses ( $I$ ).

the vacuum level at  $\sim 7$  GHz. The entire cabling is represented in Fig. 7. The signal from the sample is fed via mostly superconducting coaxial cables and two isolators into the low-noise amplifier at 4 Kelvin stage of the cryostat. A band pass microwave filter (BPF) is used to cut noise outside the isolator band.

We will turn the discussion to the room-temperature instrumentation as shown in Fig. 8. At the input side, the two pump tones from two low-phase noise microwave sources are combined with a power splitter. A tunable notch filter from Wainwright Instruments at the signal input at room temperature provides about 50 dB rejection ratio at the pump frequencies as compared to the center frequency  $\omega_c$ , and is meant to clean the phase noise of the pump sources. The phase noise would appear as an increased thermal noise  $n_i$  to the cavity, limiting the performance. Without the

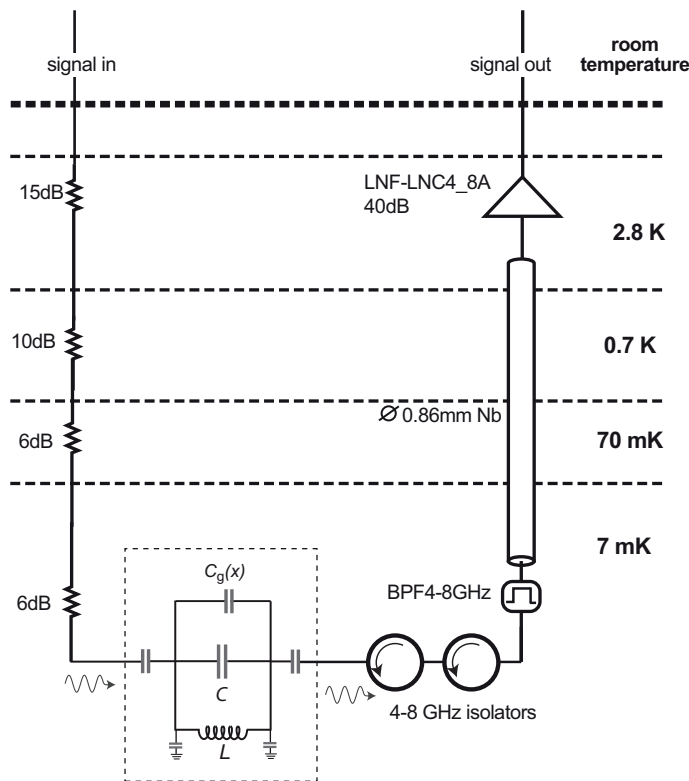


FIG. 7: Setup for the cryogenic microwave measurements.

filter, indeed, there is noticeable heating of the cavity at the highest used pump powers.

The input signal is further split, and one branch is used to create the local oscillator (LO) at the center frequency which is phase-coherent with both the two pumps. The branch for LO creation is marked in Fig. 8 as the shaded box. The signal is squared which creates a tone at  $2\omega_c$ , then filtered around this frequency in order to block unintended tones at  $2\omega_c \pm 2\omega_m$ . The frequency prescaler ADF5000BCPZ then creates the desired tone at  $\omega_c$ . It is attenuated to a suitable amplitude before being summed up to the signal from the sample, to be fed to the signal analyzer.

At room temperature, the signal coming from the sample is first further amplified by 30 dB, then band-pass filtered within the bandwidth of 4 MHz around the cavity frequency. This filtering both acts as an antialiasing filter for the digitizer, as well as attenuates the pump tones by 15-20 dB to avoid saturation of the next stages.

The vector network analyzer (VNA) is used to monitor the cavity response and hence enable for example correcting for occasionally observed drift in the cavity frequency.

We use Anritsu MS2830A signal analyzer which digitizes the datastream at 2 MHz bandwidth for the duration of approximately 1 second, and automatically makes the conversion into IQ data which is sent to computer. At the computer, we first extract the phase of the LO marker signal from the time-domain data at about 10 ms time resolution, and use this information, first of all, to make small corrections to the data due to phase drift. We construct the quadrature spectra as follows. The IQ data is converted into real-valued time-domain data as

$$I(t) = |IQ(t)| \cos(\arg(IQ(t))),$$

$$Q(t) = |IQ(t)| \sin(\arg(IQ(t))).$$

These quadratures are Fourier-transformed. We then construct a set of phase-rotated frequency-domain datasets as

$$S_{V,\Theta}(\omega) \equiv I_{\Theta}(\omega) = \cos(\Theta)I(\omega) - \sin(\Theta)Q(\omega).$$

The final result of the processing is the quadrature spectrum  $|S_{V,\Theta}(\omega)|^2$ .

The homodyne detection together with the fact that the peaks are centered at the LO frequency, cause that only one side of the *quadrature* spectra peaks are observable. For convenience, we however plot the data mirrored in about

the center frequency. In the plots the data points do not appear symmetrically situated, however, which is due to a moving average filtering applied. We cannot know if the original quadrature spectra are symmetric, however, the fact that the total output spectrum (the BG mode) is symmetric about the center frequency, as well as the theoretical prediction, indicate this is the case.

For obtaining the total spectra for the BG mode, or in case of sideband cooling, we directly process the spectrum as

$$S_V(\omega) = |\text{fft}[IQ(t)]|^2 .$$

All the instruments are locked into a common 10 MHz Rubidium frequency standard. We noticed that the Ru clock improves the phase stability by about 20 dB as compared to using a quartz clock, substantially easing the digital processing.

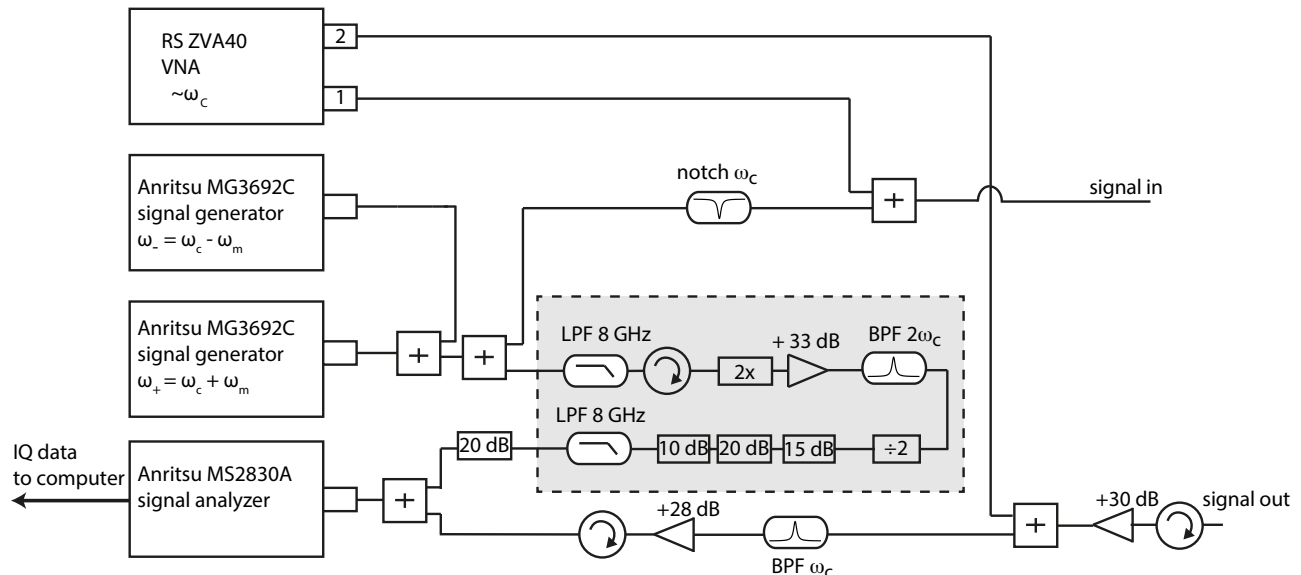


FIG. 8: Setup for the room-temperature microwave measurements. For discussion, see text.

It is important to prevent the LO signal at  $\omega_c$  from entering the sample, because it would add a drive to the mechanics. We noticed that several loose connectors can be enough to allow for this tone to pass to the sample as a crosstalk through air. In this case we could see an enhanced temperature of the mechanics if the LO generation was switched on. In the final setup, this problem disappeared.

Since we are not using a nearly quantum-limited Josephson parametric amplifier, the signal-to-noise is often much smaller than one. This leads to the issue that data recording takes long time, which causes the signal level to be sensitive to drifts of the total gain of the amplification chain. Because the vertical scale of the output spectra needs to be known accurately, it is imperative to make sure gain drifts are taken care of. To this end, while taking the quadrature spectra, instead of averaging one curve for a long time, we go through measuring a set of curves each with a different pump power. At a time, we record one curve for about 2 seconds. Before switching to the next one, we run two calibrations. The first is a measurement of the background, namely, switching all pumps off and recording the amplifier noise spectrum over the same band. This allows neutralizing gain drifts. The second is the regular sideband cooling which basically sets the gain value after drifts have been cut off.

## THEORETICAL MODELING

The cavity is described by the annihilation and creation operators  $a$  and  $a^\dagger$ , and the mechanical resonator similarly by  $b$  and  $b^\dagger$ . We use the quadratures of the mechanics

$$\begin{aligned} X_1 &= b^\dagger + b \\ X_2 &= i(b^\dagger - b) , \end{aligned} \tag{3}$$

or the other way round:

$$\begin{aligned} b &= \frac{1}{2} (X_1 + iX_2) \\ b^\dagger &= \frac{1}{2} (X_1 - iX_2) . \end{aligned} \quad (4)$$

Involving an arbitrary quadrature angle  $\Theta$ , one can write

$$X_\Theta = b^\dagger \exp(i\Theta) + b \exp(-i\Theta) . \quad (5)$$

Similar relations of course hold for the cavity operators which we do not write explicitly.

### Basic Hamiltonian

The Hamiltonian of the system consisting of the radiation-pressure coupled cavity and the mechanical resonator is

$$H = \omega_c A^\dagger A + \omega_m b^\dagger b + g_0 A^\dagger A x . \quad (6)$$

The uppercase cavity operators  $A$  and  $A^\dagger$  involve both the quantum fluctuations described by the operators  $a$  and  $a^\dagger$ , as well as the rotating classical fields due to the two pumps:

$$A = \alpha_- \exp(i\omega_- t) + \alpha_+ \exp(i\omega_+ t) + a . \quad (7)$$

The quantities  $\alpha_+$ ,  $\alpha_-$  are the classical intra-cavity amplitudes. We can, without loss of generality, suppose that they are both real. A phase difference between the amplitudes would only shift the phase reference of the quadratures.

We transform to the interaction picture with

$$U = \exp(i\omega_c t a^\dagger a) \exp(i\omega_m t b^\dagger b) . \quad (8)$$

In accord to usual practice, we neglect higher-order terms in the fluctuation operators in what follows. This amounts to linearization owing to  $|\alpha_\pm| \gg a$ . The coupling term becomes

$$\begin{aligned} &G_-^* b \exp(i(\omega_c - \omega_- + \omega_m)t) a + G_+^* b \exp(i(\omega_c - \omega_+ + \omega_m)t) a + \\ &G_- b \exp(i(\omega_- - \omega_c + \omega_m)t) a^\dagger + G_+ b \exp(i(\omega_+ - \omega_c + \omega_m)t) a^\dagger + \\ &+ G_-^* b^\dagger \exp(i(\omega_c - \omega_- - \omega_m)t) a + G_+^* b^\dagger \exp(i(\omega_c - \omega_+ - \omega_m)t) a + \\ &G_- b^\dagger \exp(i(\omega_- - \omega_c - \omega_m)t) a^\dagger + G_+ b^\dagger \exp(i(\omega_+ - \omega_c - \omega_m)t) a^\dagger . \end{aligned} \quad (9)$$

Selecting the exact co-resonance  $\omega_- = \omega_c - \omega_m$ ,  $\omega_+ = \omega_c + \omega_m$  simplifies Eq. (9) to

$$\begin{aligned} &G_-^* b^\dagger a + G_+^* b a + G_- b a^\dagger + G_+ b^\dagger a^\dagger + G_+ b a^\dagger \exp(i2\omega_m t) + \\ &+ G_- b a \exp(i2\omega_m t) + G_+^* b^\dagger a \exp(-i2\omega_m t) + G_- b^\dagger a^\dagger \exp(-i2\omega_m t) . \end{aligned} \quad (10)$$

We are working in the good-cavity limit  $\omega_m/\kappa \simeq 20 \gg 1$ , and hence we neglect the terms rotating at  $2\omega_m$  which are suppressed by nearly 40 dB.

We obtain that the Hamiltonian of the double-pumped system can be written as a beam-splitter between the cavity and the Bogoliubov modes:

$$H = a^\dagger (G_- b + G_+ b^\dagger) + a (G_-^* b^\dagger + G_+^* b) = G_\beta (a^\dagger \beta + a \beta^\dagger) , \quad (11)$$

where

$$\begin{aligned} G_\beta &= \sqrt{G_-^2 - G_+^2} \\ \beta &= b \cosh r + b^\dagger \sinh r \\ \tanh r &= G_+/G_- . \end{aligned} \quad (12)$$

The temperature of the BG mode is given as

$$\begin{aligned} n_{BG} &\equiv \beta^\dagger \beta = b^\dagger b u^2 + (b^\dagger)^2 u v + b^2 u v + b b^\dagger v^2 = b^\dagger b u^2 + (b^\dagger)^2 u v + b^2 u v + (b^\dagger b + 1)(u^2 - 1) = \\ &= 2b^\dagger b \cosh^2 r - b^\dagger b + \cosh r \sinh r ((b^\dagger)^2 + b^2) + \sinh^2 r . \end{aligned} \quad (13)$$

At low effective couplings, the phase-sensitive correlations vanish, and we get

$$n_{BG} = b^\dagger b (\cosh^2 r + \sinh^2 r) + \sinh^2 r . \quad (14)$$

### Parametric modulation

On top of the ideal model in section , we consider two additional effects, namely, a possible parametric modulation to the mechanics or to the cavity. Turns out the latter is critical for explaining the *quadrature* spectra, whereas the former does not play a significant role. The former was investigated in detail by Suh *et al.* [23], who found that it can be a serious limitation in the double pump scheme if it is strong enough to cause parametric instability.

In general, the double pump scheme is prone to issues due to unintended parametric modulation. Said briefly, this is because mixing products of the pumps at  $\omega_c \pm \omega_m$  can appear both at  $2\omega_m$  as well as  $2\omega_c$ , the frequencies most susceptible to cause parametric effects. Although a field rotating at a double frequency does not itself cause parametric modulation, it can do so via a thermal effect [23].

#### Mechanics

In the scheme, there is an unavoidable parametric modulation resulting from the second-order optomechanical coupling with the coupling coefficient  $g_2 = \frac{\partial^2 \omega_c}{\partial x^2} = \frac{\omega_c}{2C} \frac{\partial^2 C_g}{\partial x^2}$ .

The Hamiltonian Eq. (6) is added with

$$H_2 = \frac{1}{2} g_2 A^\dagger A x^2 = \frac{1}{2} g_2 A^\dagger A (b^2 + 2b^\dagger b + (b^\dagger)^2). \quad (15)$$

By the ansatz in Eq. (7) in the rotating frame, this becomes in the RWA

$$\hat{H}_2 = g_2 (|\alpha_-|^2 + |\alpha_+|^2) b^\dagger b + \frac{1}{2} g_2 \alpha_- \alpha_+ b^2 + \frac{1}{2} g_2 \alpha_+ \alpha_- (b^\dagger)^2 = G_2 b^\dagger b + \frac{1}{2} \epsilon_m b^2 + \frac{1}{2} (b^\dagger)^2, \quad (16)$$

where

$$\begin{aligned} G_2^\pm &\equiv \sqrt{g_2} \alpha_\pm = \sqrt{g_2} G_\pm / g_0 \\ G_2 &\equiv (G_2^+)^2 + (G_2^-)^2 \\ \epsilon_m &= G_2^+ G_2^- = g_2 G_- G_+ / g_0^2 \end{aligned} \quad (17)$$

The strength of the parametric modulation is hence given by the quantity  $\epsilon_m$ . In our scheme,  $g_2/(2\pi)^2 \sim 2 \times 10^{-5} \text{ Hz}^2$ . We obtain that at the highest pump powers used in the experiment,  $\epsilon_m/2\pi \simeq 300 \text{ Hz}$  which is similar to the mechanical damping rate, and hence looks like we are close to a parametric instability. However, we find that the sideband cooling interaction counteracts parametric modulation, and that the mechanical parametric modulation has a vanishing effect for either the quadrature temperatures or output spectra for  $\epsilon_m/2\pi \lesssim 10 \text{ kHz}$ .

Apart from the second-order coupling in Eq. (15), parametric modulation of the mechanical frequency could arise from thermal effects [23], with a substantially larger amplitude. We cannot qualitatively analyze this because we do not know the thermal picture well, however, we find numerically that the output quadrature spectra would be affected in a way which is inconsistent with the measurement. The peaks in the spectra would sharpen up from the ideal case and would sometimes show a multi-peak structure. This conclusion holds also if we set an arbitrary phase (see below) to the parametric modulation.

Hence, parametric modulation of the mechanical frequency in the experiment is rather well excluded.

#### Cavity

In the ideal model together with Eq. (15), parametric modulation of the cavity, or fields rotating at  $2\omega_c$ , do not arise. However, nonlinearities in the cavity, such as a Kerr effect,  $\omega_c \Rightarrow \omega_c (1 + K a^\dagger a)$ , would induce fields at  $2\omega_c$ . The existence of such nonlinearities is evidenced by the fact that frequencies of microfabricated cavities usually show a strong temperature and energy dependence. This is well known in the superconducting qubit community, and commonly thought to arise from two-level system losses.

We suppose the cavity frequency parametric modulation is a thermal effect, and the model hence, with an amplitude  $\epsilon_c$  and a possible phase shift  $\varphi$ , is

$$H_{c2} = \epsilon_c \cos(2\omega_c t + \varphi) (a^2 + (a^\dagger)^2) = \epsilon_c [\cos(\varphi) - i \sin(\varphi)] a^2 + \epsilon_c [\cos(\varphi) + i \sin(\varphi)] (a^\dagger)^2 \equiv \epsilon_c a^2 + \epsilon_c^* (a^\dagger)^2. \quad (18)$$

Here we also defined the complex modulation amplitude  $\epsilon_c$ .

### Input-output modeling

The model for the transmission setup is depicted in Fig. 6. The following modeling is basically standard input-output theory. The asymmetric cavity has the input side where the pumps are applied, with the corresponding input coupling rate  $\kappa_{Ei}$ . Energy inside the cavity can dissipate in three separate channels. One is through the input coupler. Another channel is the cavity internal losses at the rate  $\kappa_I$ , and the third is the output coupler with the rate  $\kappa_{Eo} \gg \kappa_{Ei}$ . The latter property enables us to catch nearly twice the signal as compared to a symmetric cavity, important for the integration time needed in the measurements.

The input fields to the cavity are the standard input-output theory quantum fields described by the operators  $a_{in,i}$ ,  $a_{in,o}$ ,  $a_{in,I}$  for the input and output couplers, and internal losses, respectively. They have the frequency-domain correlators ( $n = i, o, I$ )

$$\begin{aligned}\langle a_{in,n}^\dagger(\omega)a_{in,n}(-\omega) \rangle &= n_n(\omega_c) \\ \langle a_{in,n}(\omega)a_{in,n}^\dagger(-\omega) \rangle &= (1 + n_n(\omega_c)),\end{aligned}\tag{19}$$

other correlators being zero.

The three baths in general have unequal temperatures  $T_n$  which give the individual Bose factors

$$n_n(\omega_c) = (\exp(\hbar\omega_c/k_B T_n) - 1)^{-1}.\tag{20}$$

The internal losses of the mechanics are due to the field  $b_{in}$  which has similar properties as in Eq. (19), Eq. (20), with the replacements  $\omega_c \Rightarrow \omega_m$ ,  $n_n \Rightarrow n_m^T$ .

We suppose the  $i$  and  $o$  baths are at zero temperature which is rather standard assumption. We also have carefully taken care to isolate excess noise from both these ports. The fact that the thermal calibration and sideband cooling calibration work well without a dip arising from such noise supports this assumption. The cavity internal bath, however, rises up to  $n_I \sim 0.9$  at the highest pump powers.

The equations of motion, including for completeness the parametric modulations to both the mechanics and cavity, are

$$\begin{aligned}\dot{a} &= -i(G_- b + G_+ b^\dagger) - \frac{\kappa}{2}a - i\varepsilon_c a^\dagger + \sqrt{\kappa_{Ei}}a_{in,i}(t) + \sqrt{\kappa_{Eo}}a_{in,o}(t) + \sqrt{\kappa_I}a_{in,I}(t) \\ \dot{a}^\dagger &= i(G_-^* b^\dagger + G_+^* b) - \frac{\kappa}{2}a^\dagger + i\varepsilon_c^* a + \sqrt{\kappa_{Ei}}a_{in,i}^\dagger(t) + \sqrt{\kappa_{Eo}}a_{in,o}^\dagger(t) + \sqrt{\kappa_I}a_{in,I}^\dagger(t) \\ \dot{b} &= -iG_2 b - iG_+ a^\dagger - iG_-^* a - i\varepsilon_m b^\dagger - \frac{\gamma_m}{2}b + \sqrt{\gamma_m}b_{in} \\ \dot{b}^\dagger &= iG_2 b^\dagger + iG_+^* a + iG_- a^\dagger + i\varepsilon_m^* b - \frac{\gamma_m}{2}b^\dagger + \sqrt{\gamma_m}b_{in}^\dagger\end{aligned}\tag{21}$$

We solve the frequency-domain equations resulting from Eq. (21) numerically up to all orders. The response of each operator is written as arising from all the input fields, given as an example for the cavity operator as:

$$\begin{aligned}a(\omega) &= m(\omega)a_{in,i}(\omega) + l(\omega)a_{in,i}^\dagger(\omega) + m_o(\omega)a_{in,o}(\omega) + l_o(\omega)a_{in,o}^\dagger(\omega) + \\ &+ m_I(\omega)a_{in,I}(\omega) + l_I(\omega)a_{in,I}^\dagger(\omega) + q(\omega)b_{in}(\omega) + r(\omega)b_{in}^\dagger(\omega).\end{aligned}\tag{22}$$

One of the aims is to calculate the quadrature spectra of the mechanical resonator, in particular, the fluctuation energy as a function of the quadrature angle  $\Theta$ . The spectra of the mechanics is given as

$$\begin{aligned}S_{x,\Theta}(\omega) &= \langle (b^\dagger(\omega) \exp(i\Theta) + b(\omega) \exp(-i\Theta))(b^\dagger(-\omega) \exp(i\Theta) + b(-\omega) \exp(-i\Theta)) \rangle = \\ &= \langle b^\dagger(\omega)b^\dagger(-\omega) \rangle \exp(2i\Theta) + \langle b^\dagger(\omega)b(-\omega) \rangle + \langle b(\omega)b^\dagger(-\omega) \rangle + \langle b(\omega)b(-\omega) \rangle \exp(-2i\Theta).\end{aligned}\tag{23}$$

The correlators are calculated using Eq. (22), Eq. (19).

The quadrature variance, directly giving the energy of the quadrature in units of the zero-point energy is given as

$$\Delta X_\Theta^2 = \frac{1}{2\pi} \int_{-\infty}^{\infty} 2S_{x,\Theta}(\omega) d\omega.\tag{24}$$

In these units, the total energy of the mode is

$$n_m = \frac{1}{4} \left( \Delta X_\Theta^2 + \Delta X_{\Theta+\pi/2}^2 \right).\tag{25}$$

For example, in the ground state this gives  $n_m = \frac{1}{2}$ .

We use the standard nomenclature that the minimum of  $\Delta X_\Theta^2$  with respect to  $\Theta$  is called the  $X_1$  quadrature, and the maximum is  $X_2$ . The corresponding variances are labeled with the shorthand notations  $\Delta X_1^2$  and  $\Delta X_2^2$ , respectively.

The final measured quantity is the output field of the field leaking out from the output coupler of the cavity, given as

$$a_{out,o} = \sqrt{\kappa E_o} a - a_{in,o}. \quad (26)$$

The spectral density of the corresponding voltage fluctuations is labeled  $S_V(\omega)$ . This is the quantity presented in the figures, given in units of quanta. The quadrature spectrum  $S_{V,\Theta}(\omega)$  of the voltage fluctuations is given as in Eq. (23) by replacing the mechanics operators with those of the output field (Eq. (26)). For notational convenience, we use for the spectra of the minimum energy and maximum energy quadratures the notations  $S_1(\omega)$  and  $S_2(\omega)$ , respectively. The final deductions regarding squeezing in the mechanical resonator are based on direct comparison of the measured phase-sensitive output spectrum to the predictions resulting from the presented formalism.

Since theoretical expectations arise from nontrivial analysis, it is integral to make sure the calculations are sound. We verified that the results of the theoretical formalism are similar to earlier work in cases where comparison is possible. More specifically, the amount of squeezing our formalism gives is the same as in Ref. 13, as well as the total output spectrum reduces to their result in the limit of small internal cavity losses. If considering only the regular sideband cooling case, analytical results are available in Ref. 29, and our analysis agrees with those results.

## DATA ANALYSIS

Here we present further data, and some details relating to the data analysis.

### Bath temperatures

In Fig. 9 we show how the baths, to which either the cavity and the mechanics are coupled, heat up as a function the pump power(s). This heating ultimately limits the squeezing. The bath temperatures are not totally monotonous with respect to increasing pump power. We also sometimes observe the bath temperatures to slightly fluctuate during a cooldown, presumably due to changes the configuration of microscopic defects in the sample, varying the thermal coupling from the pump into the bath.

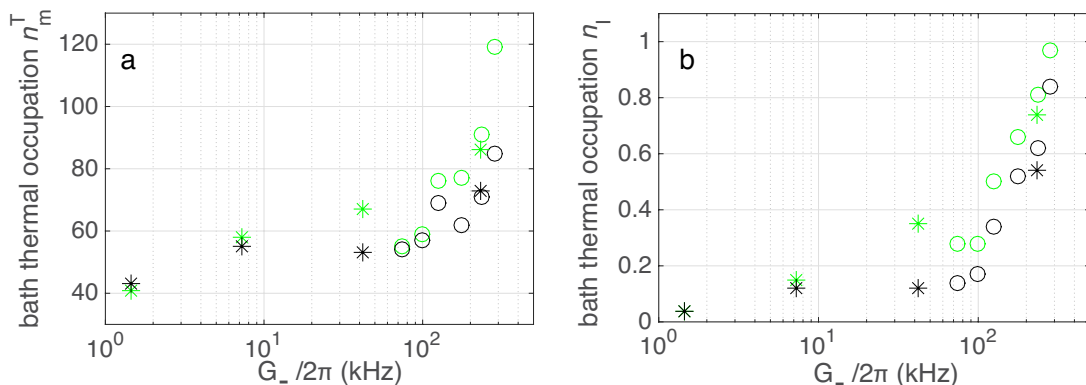


FIG. 9: *Bath temperatures as a function of effective coupling.* The data points are from the data shown in the main text in Fig. 2 (asterisk) and Fig. 3 (circles). As elsewhere, green refers to the BG mode, and black is the sideband cooling. (a), mechanics. (b), cavity.

### Phase-insensitive data

As mentioned in main text, it is possible to obtain a good fit of the Bogoliubov mode data (that is, the total output spectrum) without imposing any parametric modulation. However, one finds out that far too little phase dependence would be predicted for the quadrature spectra. We illustrate this in Fig. 10. The color codes are as in Fig. 3d in main text. The parameters are  $n_m^T = 91$ ,  $n_I = 1.07$ ,  $\Delta X_1^2 = 0.79$ . One has to use an elevated cavity internal temperature to explain the enhanced emission of BG mode. In the real case, the parametric modulation acts to boost up the emission. The squeezing is little affected, nevertheless.

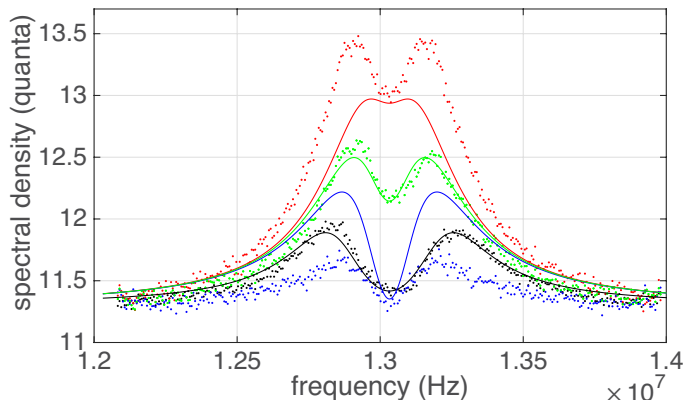


FIG. 10: *Modeling without parametric modulation.* As Fig. 3d in main text, but with  $\epsilon_c = 0$ .

### Error analysis

Next we discuss the error analysis of the final results demonstrating squeezing. A general remark is that the shapes of the BG mode and quadrature spectra are sensitive to most parameters, the bath temperatures of both the mechanics and the cavity in particular. The third parameter on which squeezing significantly depends on and whose independent determination has non-negligible error margins, is the mechanical intrinsic linewidth  $\gamma_m$ .

We make error estimate for the squeezed quadrature variance using standard error propagation as

$$\delta(\Delta X_1^2) = \sqrt{\sum_i \left( \delta y_i \frac{\partial \Delta X_1^2}{\partial y_i} \right)^2}, \quad (27)$$

where the statistical uncertainties of variables  $y_i$  are marked by  $\delta y_i$ . We do not have an analytical theory which would allow for rigorously obtaining  $\delta y_i$ 's from the final fitting results. We use the following approach, treating as the sources of uncertainty the mentioned three parameters  $y_i = [n_I, n_m^T, \gamma_m]$ .

The uncertainty  $\delta n_m^T$  of the starting temperature of the mechanics bath is particularly important to consider. At low pump powers, an error in the bath temperature calibration would show up as a scaling factor in the Lorentzian peak, easily going unnoticed. The real situation, however, is better because towards the strong-coupling regime, the starting temperature has a more complicated influence than just scaling the peaks.

We estimate  $\delta n_m^T$  from the scatter of the data points in Fig. 2 a in main text at  $T < 20$  mK which region marks the base temperature, but where the temperature reading shows some fluctuations. The standard error of the mean gives  $\delta n_m^T \simeq 3$ , or approximately 10 % uncertainty.

The uncertainty of the fitted value of  $\gamma_m$  in the data shown in Fig. 1e in main text is  $\delta \gamma_m / 2\pi \simeq 14$  Hz.

The uncertainty of  $n_I$  is not as straightforward, but can be obtained from fitting an analytical formula from Ref. 29 to the BG mode data which is a rather good approximation. The uncertainty of the fitted value gives  $\delta n_I \simeq 0.08$ .

Numerically we obtain the derivatives

$$\frac{\partial \Delta X_1^2}{\partial n_m^T} \simeq 0.0043,$$

$$\frac{\partial \Delta X_1^2}{\partial \gamma_m} \simeq 0.0011,$$

$$\frac{\partial \Delta X_1^2}{\partial n_I} \simeq 0.22,$$

which do not significantly depend on the specific parameter values.

Combining,

$$\delta(\Delta X_1^2) \simeq 0.08, \quad (28)$$

which is the final uncertainty estimate.

We can also demonstrate that the theory curves are rather sensitive to the parameters. In Fig. ?? we show plots as in Fig. 3 d in main text, but one of the important parameters is intentionally offset by 20 % from the nominal value to the direction which degrades squeezing, while other parameters are kept unchanged. In each case, the agreement is clearly worsened, while squeezing is affected around 10 %.

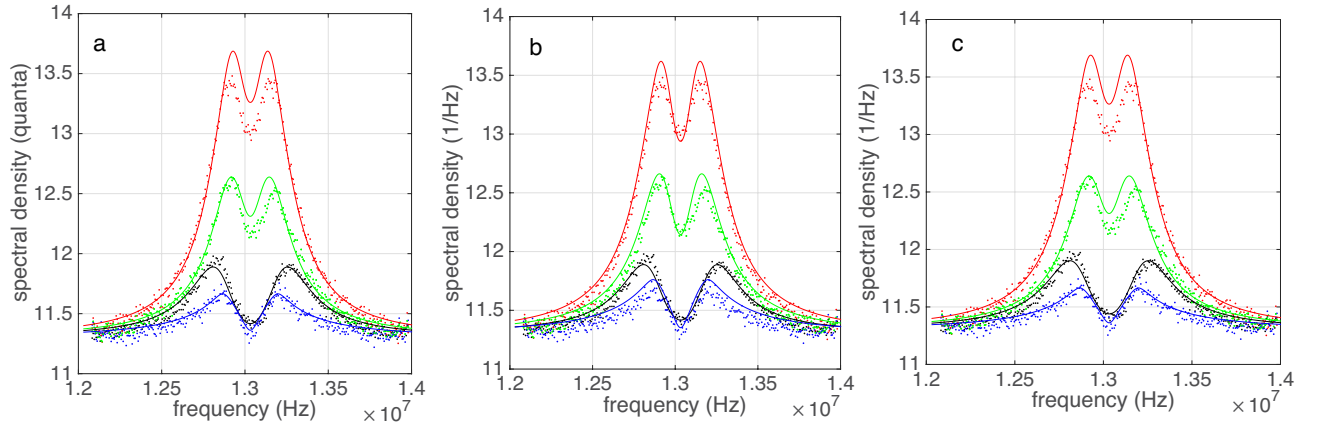


FIG. 11: Tests of sensitivity to parameters. (a),  $n_m^T = 109$ , (b),  $n_I = 0.97$ , (c),  $\gamma_m/2\pi = 396$  Hz.